Dalton Transactions

Accepted Manuscript

This is an *Accepted Manuscript*, which has been through the RSC Publishing peer review process and has been accepted for publication.

Accepted Manuscripts are published online shortly after acceptance, which is prior to technical editing, formatting and proof reading. This free service from RSC Publishing allows authors to make their results available to the community, in citable form, before publication of the edited article. This *Accepted Manuscript* will be replaced by the edited and formatted *Advance Article* as soon as this is available.

To cite this manuscript please use its permanent Digital Object Identifier (DOI®), which is identical for all formats of publication.

More information about *Accepted Manuscripts* can be found in the **Information for Authors**.

Please note that technical editing may introduce minor changes to the text and/or graphics contained in the manuscript submitted by the author(s) which may alter content, and that the standard **Terms & Conditions** and the **ethical guidelines** that apply to the journal are still applicable. In no event shall the RSC be held responsible for any errors or omissions in these *Accepted Manuscript* manuscripts or any consequences arising from the use of any information contained in them.

Cite this: DOI: 10.1039/c0xx00000x

www.rsc.org/xxxxxx

ARTICLE TYPE

Spin-Crossover Phenomena of Mononuclear Mn^{III} Complex Tuned by Metal Dithiolene Counteranions

Ying Chen,[a] Fan Cao,[a] Rong-Min Wei,[a] Yang Zhang,[a] Yi-Quan Zhang*[b] and You Song*[a]

Received (in XXX, XXX) Xth XXXXXXXXX 200X, Accepted Xth XXXXXXXXX 200X
DOI: 10.1039/b000000x

Three ion-pair complexes based on spin-crossover $[Mn(5\text{-Br-sal-N-1,5,8,12})]ClO_4$ with $TBA_2[Ni(mnt)_2]$, $TBA_2[Pt(mnt)_2]$ (mnt = maleonitriledithiolate) and $TBA[Ni(dmit)_2]$ respectively (dmit = 2-thioxo-1,3-dithiole-4,5-dithiolato) have been synthesized and structurally characterized. Complexes **1** $[Mn(5\text{-Br-sal-N-1,5,8,12})]_2[Ni(mnt)_2]$ and **2** $[Mn(5\text{-Br-sal-N-1,5,8,12})]_2[Pt(mnt)_2]$ are isomorphic and show the axial compression of the octahedral coordination environment of Mn^{III} ions. With the temperature increasing the equatorial metal-ligand bond lengths show significant elongation, but the axial bond lengths remain unchanged. Complex **3** $[Mn(5\text{-Br-sal-N-1,5,8,12})][Ni(dmit)_2]\cdot CH_3CN$ contains π-π, p-π and H-bonds weak interactions. Magnetic investigation shows the spin-crossover phenomena for **1** and **2**, and $T_{1/2}$ has been increased 230 K comparing with the reactant complex. However, no spin-crossover was observed in complex **3**, and theoretical calculations show that there are weak antiferromagnetic couplings mediated through π-π interactions.

Introdction

When a molecular species contain an octahedrally coordinated transition metal ion with $3d^n$ (n = 4 to 7) configuration, by applying external stimuli,[1-4] they may exhibit a transiton between a low-spin (LS) and a high-spin (HS) state. If this transition is abrupt and show thermal hysteresis, this kind of molecular materials have great potential application on memory devices.[5] Furthermore, this so-called spin-crossover (SCO) phenomenon is a representative example of molecular bistability,[6] so based on this nature SCO complexes could also be used as thermal sensors and molecular switches. Therefore, in the study of magnetic properties, SCO phenomena has attracted much attention over the past decades.

On the other hand, in the study of magnetic properties of coordination complexes, the research on organic and organometallic redicals[7-10] has increasingly become an important field as a result of their spectacular properties.[11-13] For example, organic redical crystals 1,3,5-trithia-2,4,6-triazapentalenyl[14] display magnetic bistability with a wide thermal hysteresis loop over the temperature range 230 to 305 kelvin. And, metal bis-1,2-dithiolene complexes, as organic donors and acceptors, possess a delocalized electron system as a planar central core $M(C_2S_2)_2$ and present different formal oxsidation states.[15] This series of complexes have been intensively studied as the component molecular conductors. In addition, metal dithiolene complexes embrace rich physical properties, such as Peierls instability of the low-dimensional systems,[16] the qunantum fluctuations (the cause of the quantum spin liquid[17]), the charge separation, and so forth. Consequently, both SCO and metal dithiolene complexes could undergoes phase transition, thus, combining two components together might give rise to novel molecular materials with exotic phenomenon. It is worth noting that Oshio and co-workers reacted magnetic bistable $[Fe(dpp)_2](BF_4)_2$[18] with $TBA[Ni(mnt)_2]$ get a complex $[Fe(dpp)_2][Ni(mnt)_2]_2\cdot MeNO_2$,[19] which shows multiple bistability and tristability. Faulmann's group has devoted a lot of work on combining SCO and electricity conductivity.[20-24] Particularly, they combined $[Ni(dmit)_2]^-$ with the spin equilibrium $[Fe(sal_2\text{-trien})]^+$,[25] obtaining a complex $[Fe(sal_2\text{-trien})][Ni(dmit)_2]$, which shows cooperative spin transition behaviour with a wide hysteresis loop (30 K).[21] It seems that metal dithiolene anions could influence SCO properties in a great degree. In fact, intermolecular weak contact like π-π interactions plays a key role in cooperativity of an SCO behavior.[26,27] Herein, we chose an ambient stable complex $[Mn(5\text{-Br-sal-N-1,5,8,12})]ClO_4$[28] with spin-crossover property, and hybridized it with $TBA_2[Ni(mnt)_2]$, $TBA_2[Pt(mnt)_2]$ and $TBA[Ni(dmit)_2]$, respectively, obtaining three ion-pair complexes, in which **1** and **2** show SCO phenomena with higher conversion temperature, but **3** exhibits weak antiferromagnetic interaction between anion and cation by means of π-π interactions without SCO property any longer.

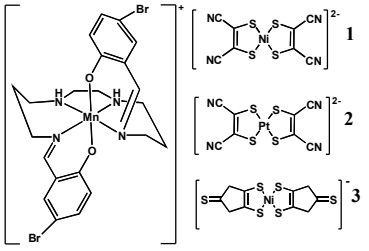

Scheme 1 Scheme view of the $[Mn(5\text{-Br-sal-N-1,5,8,12})]^+$, $[Ni(mnt)_2]^{2-}$, $[Pt(mnt)_2]^{2-}$, and $[Ni(dmit)_2]^-$ units.

Dalton Transactions Accepted Manuscript

Table 1 Crystal structural data and refinement parameters for **1** and **3**.

Complex			**1**			**3**
Chemical formula			$C_{52}H_{52}Br_4Mn_2N_{12}NiO_4S_4$			$C_{30}H_{29}Br_2MnN_5NiO_2S_{10}$
Temperature/K	123(2)	296(2)	350(2)	400(2)	473(2)	296(2)
Fw / g mol^{-1}	1525.53	1525.53	1525.53	1525.53	1525.53	1085.65
Crystal system	Triclinic	Triclinic	Triclinic	Triclinic	Triclinic	Triclinic
Space group	$P\bar{1}$	$P\bar{1}$	$P\bar{1}$	$P\bar{1}$	$P\bar{1}$	$P\bar{1}$
a/Å	8.1908(9)	8.2849(5)	8.308(2)	8.3414(15)	8.381(3)	10.9060(9)
b/Å	9.9971(11)	10.0345(6)	10.025(2)	10.0287(18)	10.044(3)	12.1826(10)
c/Å	18.358(2)	18.4775(10)	18.528(5)	18.604(3)	18.692(6)	16.1265(13)
α/°	78.0250(10)	78.3540(10)	78.414(4)	78.537(3)	78.624(6)	94.2340(10)
β/°	79.554(2)	79.2600(10)	79.045(4)	78.887(3)	78.750(6)	104.1830(10)
γ/°	83.196(2)	84.2090(10)	84.969(4)	85.589(3)	86.181(6)	92.672(2)
Unit cell volume/Å^3	1441.0(3)	1474.95(15)	1482.3(6)	1495.4(5)	1512.2(9)	2067.0(3)
Z	1	1	1	1	1	2
ρ_{calcd} / mg m^{-3}	1.758	1.717	1.709	1.694	1.675	1.744
μ/mm^{-1}	3.729	3.643	3.625	3.593	3.553	3.235
Reflections measured	11687	10098	11045	10930	11203	11697
Independent reflections	5592	6708	5141	5165	5233	7231
R_{int}	0.0384	0.0221	0.0572	0.0684	0.0706	0.0202
R_1 (all data)	0.0450	0.0689	0.0824	0.0873	0.1222	0.0543
wR_2 (all data)	0.1329	0.1387	0.1777	0.1352	0.1348	0.0930
GOF on F^2	1.005	1.001	1.036	0.996	0.997	1.001

The temperature-dependent measurements were carried out on the same single crystal.

Experimental

Physical measurements

Spectra, TA and magnetic properties. The IR spectrum were carried out with a Nexus 870 FT-IR spectrometer using KBr pellets in the range of 400-4000 cm^{-1}. Elemental analyses of C, H, N were recorded on a PerkinElmer 240C elemental analyzer. The data of magnetic properties for crystalline samples was obtained on Quantum Design SQUID MPMS-XL7 magnetometer in the temperature range 1.8 ~ 350K and on Quantum Design SQUID MPMS-XL5 magnetometer in the range of 300 K ~ 525 K for **1** and 300 K ~ 540 K for **2** under a applied magnetic field of 2000 Oe. Thermal analysis was perfomed with PerKinElmer Pyris 1 DSC calorimeter in the temperature range 20 to 670 ºC.

Crystal structure determination. The crystal sturctures were determined on a Bruker SMART diffractometer equipped with a CCD type area detector. The data was collected with graphite monochromated Mo-Kα radiation (λ = 0.71073 Å) at 123 K, 296 K, 350 K, 400 K and 473K. All absorption corrections were performed by using SADABS[29] program supplied by Bruker. The sturctures were solved by Patterson method [30] and refined by full-matrix least-squares on all F^2 data using the program SHELXL-97.[31] All non-hydrogen atoms were refined anisotropically and the hydrogen atoms were included in calculated positions and refined isotropically.

Synthesis

Starting meterials. All of the reagents and chemicals were analytically pure, purchased from commercial sources and were used without further purification. Complexes [Mn(5-Br-sal-N-1,5,8,12)]ClO_4,[28] $TBA_2[M(mnt)_2]$ (M = Ni, Pt)[32] and TBA[Ni(dmit)$_2$] [33] were prepared by literature procedures.

Preparation of [Mn(5-Br-sal-N-1,5,8,12)]$_2$[Ni(mnt)$_2$] (1) A solution of 34.6 mg (0.05 mmol) [Mn(5-Br-sal-N-1,5,8,12)]ClO_4 in 20 mL methanol is added, with stirring, to a solution of 20.6 mg (0.025 mmol) $TBA_2[Ni(mnt)_2]$ in 20 mL acetonitrile, kept the dark red solution stirring for five minutes, then filtered, and stayed the filtrate for about one week, black plate-like crystals suitable for X-ray diffraction were grown and collected by filtration carefully (yield 78.68%). Anal. Caled. for $C_{26}H_{26}N_6O_2S_2MnBr_2Ni_{0.5}$: C, 40.94; H, 3.44; N, 11.02. Found: C, 40.89; H, 3.58; N, 10.92. IR spectrum (KBr, cm^{-1}): $\nu_{C\equiv N}$ of $[Ni(mnt)_2]^{2-}$, 2193.8(s), 2210.3(sh); $\nu_{C=C}$ of benzene ring, 1614.6(s), 1526.0(s), 1452.8(s).

Preparation of [Mn(5-Br-sal-N-1,5,8,12)]$_2$[Pt(mnt)$_2$] (2) The synthetic procedure for complex **2** is analogous to that of **1** but using $TBA_2[Pt(mnt)_2]$ instead of $TBA_2[Ni(mnt)_2]$. From the result dark red solution, black plate-like crystals suitable for X-ray diffration were grown in about one week on standing at ambient temperature (yield 81.26%). Anal. Caled. for $C_{26}H_{26}N_6O_2S_2MnBr_2Pt_{0.5}$: C, 37.58; H, 3.15; N, 10.11. Found: C, 37.31; H, 3.31; N, 10.05. IR spectrum (KBr, cm^{-1}): $\nu_{C\equiv N}$ of $[Pt(mnt)_2]^{2-}$, 2195.9(s), 2183.1(sh); $\nu_{C=C}$ of benzene ring, 1614.5(s), 1526.4(s), 1453.3(s).

Preparation of [Mn(5-Br-sal-N-1,5,8,12)][Ni(dmit)$_2$]·CH$_3$CN (3) A solution of 17.3 mg (0.025 mmol) [Mn(5-Br-sal-N-1,5,8,12)]ClO_4 in 10 mL acetonitrile is added, with stirring, to a solution of 17.3 mg (0.025 mmol) TBA[Ni(dmit)$_2$] in 10 mL actone-acetonitrile (1:1 v/v), kept the green solution stirring for five minutes, then filtered, and stayed the filtrate for about ten days, dark green long-strip crystals suitable for X-ray diffraction formed and were collected by filtration carefully (yield 56.30%). Anal. Caled. for $C_{30}H_{29}N_5O_2S_{10}MnBr_2Ni$: C, 33.19; H, 2.69; N, 6.45. Found: C, 33.01; H, 2.77; N, 6.23. IR spectrum (KBr, cm^{-1}): $\nu_{C=C}$ of benzene ring, 1452.2(s); $\nu_{C=S}$ of $[Ni(dmit)_2]^{2-}$, 1058.8(s). TA: at about 195 ºC the sample lost 7.3098% weight.

Computational details

Theoretical calculations were used to evaluate the exchange coupling constant and magnetic anisotropy for complex **3**. To obtain the isotropic exchange coupling constant J, Orca 2.9.1 calculations[34] were performed with the popular hybrid functional B3LYP proposed by Becke[35-36] and Lee et al.[37] Triple-ζ with one polarization function def2-TZVP[38] basis set was used for all atoms, and the scalar relativistic treatment (ZORA) was used in

Dalton Transactions Accepted Manuscript

Table 2 Selected bond lengths (Å) and angles (°) for **1**.

	123K	296K	350K	400K	473K
			Bond Lengths (Å)		
Mn(1)-O(1)	1.885(2)	1.878(3)	1.885(3)	1.888(2)	1.881(4)
Mn(1)-O(2)	1.881(3)	1.869(2)	1.881(3)	1.875(2)	1.881(4)
Mn(1)-N(1)	1.984(3)	2.020(3)	2.031(3)	2.065(3)	2.084(4)
Mn(1)-N(2)	2.038(3)	2.071(3)	2.094(3)	2.109(3)	2.122(5)
Mn(1)-N(3)	2.048(3)	2.091(3)	2.108(3)	2.145(3)	2.162(5)
Mn(1)-N(4)	1.987(3)	2.016(3)	2.034(3)	2.054(3)	2.065(5)
Ni(1)-S(1)	2.1716(10)	2.1697(12)	2.1670(12)	2.1695(11)	2.1686(17)
Ni(1)-S(2)	2.1824(9)	2.1882(11)	2.1786(11)	2.1829(10)	2.1818(18)
			Bond Angles (°)		
O(2)-Mn(1)-O(1)	179.87(13)	179.18(11)	178.52(11)	177.80(10)	177.51(15)
O(2)-Mn(1)-N(4)	89.02(11)	88.65(11)	88.16(11)	87.25(10)	87.25(17)
O(1)-Mn(1)-N(4)	91.07(12)	90.90(12)	90.95(12)	91.35(10)	91.22(18)
O(2)-Mn(1)-N(1)	90.67(12)	91.02(12)	90.97(12)	90.93(10)	91.25(17)
O(1)-Mn(1)-N(1)	89.23(11)	88.36(12)	88.02(12)	87.69(10)	87.17(17)
N(4)-Mn(1)-N(1)	95.30(12)	97.34(13)	99.75(12)	101.34(11)	102.82(18)
O(2)-Mn(1)-N(2)	88.47(11)	88.74(12)	89.30(12)	89.88(10)	89.91(18)
O(1)-Mn(1)-N(2)	91.45(12)	91.78(13)	91.74(12)	91.78(10)	91.95(19)
N(4)-Mn(1)-N(2)	173.98(12)	172.80(14)	171.46(12)	170.06(11)	169.25(19)
N(1)-Mn(1)-N(2)	90.21(12)	89.41(13)	88.45(12)	88.22(11)	87.6(2)
O(2)-Mn(1)-N(3)	91.09(12)	91.20(13)	91.57(12)	92.19(10)	91.98(18)
O(1)-Mn(1)-N(3)	89.00(11)	89.48(12)	89.59(12)	89.43(10)	89.91(18)
N(4)-Mn(1)-N(3)	89.37(12)	88.90(13)	88.22(13)	87.47(11)	87.04(19)
N(1)-Mn(1)-N(3)	175.04(12)	173.42(13)	171.72(13)	170.79(11)	169.77(19)
N(2)-Mn(1)-N(3)	85.20(12)	84.44(13)	83.70(13)	83.12(11)	82.7(2)
S(1)-Ni(1)-S(2)	92.02(4)	91.86(4)	91.84(4)	91.86(4)	91.53(7)
S(1)-Ni(1)-S(2A)	87.98(4)	88.14(4)	88.16(4)	88.14(4)	88.47(7)

Symmetry code : 1 − x, 2 − y, 1 − z.

all calculations. The large integration grid (grid = 6) was applied to Mn^{III} and Ni^{III} for ZORA calculations. Tight convergence criteria were selected to ensure that the results are well converged with respect to technical parameters. For each tetranuclear unit [see Figure 6(a)], we calculated the energies of two spin states: the high-spin state (E_{HS}, $S_{HS} = S_{Mn} + S_{Mn'} + S_{Ni} + S_{Ni'}$), and the low-spin state (E_{LS}, spin flip for two Ni^{III}, $S_{LS} = S_{Mn} + S_{Mn'} - S_{Ni} - S_{Ni'}$), and we could obtain the Mn^{III}-Ni^{III} coupling constant J according to the spin Hamiltonian $\mathbf{H} = -2J(\mathbf{S}_{Mn}\mathbf{S}_{Ni} + \mathbf{S}_{Mn}\mathbf{S}_{Ni'} + \mathbf{S}_{Mn'}\mathbf{S}_{Ni} + \mathbf{S}_{Mn'}\mathbf{S}_{Ni'})$, and for complex **3** the constant J can be calculated by the formula $J = (E_{LS} - E_{HS})/20$.

In the calculation of D for the Mn^{III} fragment, CASPT2 was used with MOLCAS 7.8 program package.[39] For the first CASSCF calculation, the basis sets for all atoms are atomic natural orbitals from the MOLCAS ANO-RCC library: ANO-RCC-VTZP for magnetic center ion Mn^{III}; VTZ for close O and N; VDZ for distant atoms. The calculations employed the second order Douglas-Kroll-Hess Hamiltonian, where scalar relativistic contractions were taken into account in the basis set. After that, the effect of the dynamical electronic correlation was applied using CASPT2. And then, the SOC (spin-orbit coupling) was handled separately in the RASSI module. The active space is (4, 5) Mn^{III}. The mixed spin-free states are 50 for the Mn^{III} fragment.

Results and Discussion

The cell parameters, refinement details, together with crystal data parameters are summarized in Table 1 (for complexes **1** and **3**) and Table S1 (in ESI for complex **2**). The octahedral structural parameters of Mn^{III} for $[Mn(5\text{-Br-sal-N-1,5,8,12})]ClO_4$ and complexes **1-3** are shown in Table S2 (in ESI). Selected bond distances and angles for complexes **1**, **2** and **3** are listed in Table 2, Table S3 (in ESI), and Table 3, respectively.

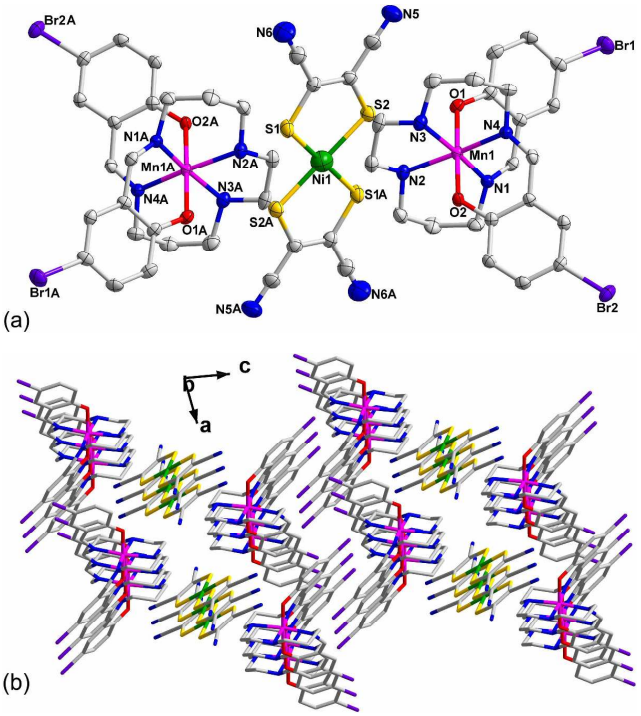

Fig. 1 (a) Ellipsoid view for complex **1** at 296K with atom labelling (except carbon atoms). Symmetry code: A = 1 − x, 2 − y, 1 − z. (b) A view along axis *b* for complex **1**. Hydrogen atoms are omitted for clarity.

Structural Description

$[Mn(5\text{-Br-sal-N-1,5,8,12})]_2[Ni(mnt)_2]$ (1) Ellipsoid view for complex **1** is displayed in Fig. 1(a). An asymmetric unit of complex **1** contains one half $[Ni(mnt)_2]^{2-}$ and one $[Mn(5\text{-Br-sal-N-1,5,8,12})]^{+}$ cation. The shown other part in the figure was

Dalton Transactions Accepted Manuscript

grown by the symmetry code 1 − x, 2 − y, 1 − z. As displayed in Fig. 1(b), the cations and anions form completely segregated stacks along *b* direction and spread out onto the *ac* plane. As shown in Fig. 2, comparing the bond lengths at five collection temperatures, all of four equatorial Mn-N bond lengths show significant elongation, but the two axial Mn-O bond lengths remain unchanged. In addition, with the rise of the temperature, the unit cell volume increases from 1441.0 $Å^3$ at 123 K to 1512.2 $Å^3$ at 473 K. In a word, the configuration of Mn^{III} in complex **1** shows an equatorial expansion with the temperature increasing in the axial compression octahedral environment. That is also be evidenced by the calculated values of average trigonal distortion angle Φ and octahedral distortion parameter Σ (Table S2), with the temperature rising, the Φ and Σ values increase (for Φ : from 1.81 at 123 K to 3.06 at 473 K; for Σ : from 19.5 at 123 K to 37.64 at 473 K). It indicates that the higer temperature is, the more significant compression of the octahedrally coordinated Mn^{III} shows. Nevertheless, it is an intermediate phase rather than high-spin phase at 473 K, which could be evidenced by following magnetic data. In the anion $[Ni(mnt)_2]^{2-}$, the Ni^{2+} ion is coordinated to four sulfur atoms and exhibits quasi-square planar geometry. The Ni1-S1 and Ni1-S2 bond distances are 2.1707(8) and 2.1850(8) Å respectively. The S-Ni-S angle is 91.88°. These results are consistent with those found in other $[Ni(mnt)_2]^{2-}$ complexes.[40,41]

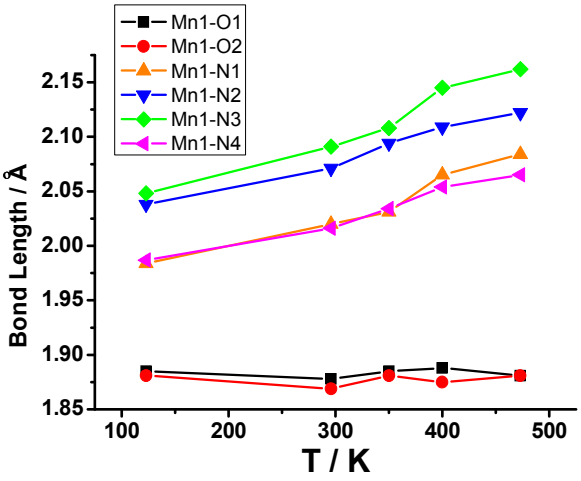

Fig. 2 Comparison of Mn—N and Mn—O bond lengths at five collection temperatures in complex **1**.

$[Mn(5\text{-Br-sal-N-1,5,8,12})]_2[Pt(mnt)_2]$ (2) Complexes **2** and **1** are isomorphic, so the structure of **2** is not described here in detail. Crystal structural data and refinement parameters for **2** are listed in Table S1 (in ESI). The calculated average trigonal distortion angle Φ and octahedral distortion parameter Σ (in Table S2) suggest the configuration of Mn^{III} in complex **2** is very close to that in complex **1**. The selected bond distances and angles at the five collection temperatures are shown in Table S3. Comparison of Mn—N and Mn—O bond lengths at five temperatures for complex **2** is displayed in Fig. S1, which shows analogous variation tendency compared with that for complex **1**. The bond lengths of Pt-S and S-Pt-S bite angles also agree well with those found in the reported $[Pt(mnt)_2]^{2-}$ complexes.[42,43]

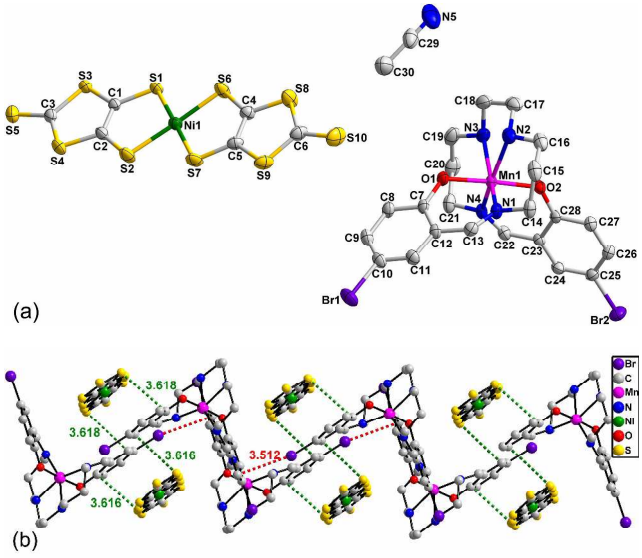

Fig. 3 (a) Ellipsoid view for complex **3** at 296 K with labelled atoms. (b) Details for π-π and p-π interactions in **3** (All of CH_3CN molecules and hydrogen atoms were omitted).

$[Mn(5\text{-Br-sal-N-1,5,8,12})][Ni(dmit)_2]\cdot CH_3CN$ (3) Fig. 2(a) displays the ellipsoid view for complex **3**. In an asymmetric unit, besides one $[Mn(5\text{-Br-sal-N-1,5,8,12})]^+$ cation and one $[Ni(dmit)_2]^-$ anion, there is also a solvent molecule CH_3CN in it, which is accordance well with the TA results (Fig. S4 in ESI). For complex **3**, Table S2 shows that the value of Φ (5.69) and Σ (83.66) greatly deviate from 0°, which can be ascribed to significant Jahn-Teller distortions. As also displayed in Fig. 4, the coordination environment of Mn^{III} in **3** shows significant geometric distortion comparing with that in **1** and **2** at 296 K. In the anion $[Ni(dmit)_2]^-$, the bond distances and angles is consisitent with the reported results.[44,45] Furthermore, there are a lot of π-π (C···S) and p-π (Br···C) interactions in complex **3**. Two isotrithione rings of a $[Ni(dmit)_2]^-$ interacts with the benzene rings of two $[Mn(5\text{-Br-sal-N-1,5,8,12})]^+$ via π-π stacking respectively. As shown in Fig. 2(b), two cations and two anions forms a repeating tetranuclear subunits via π-π interactions, and two adjacent cations $[Mn(5\text{-Br-sal-N-1,5,8,12})]^+$ interplay via p-π interactions. In addition, there are two kinds of hydrogen bonds in complex **3**, in which one is C8—H8···S10 (length, 2.87 Å; angle, 158°), the other is C22—H22···N5 (length, 2.47 Å; angle, 154°) as displayed in Fig. S6 (in ESI).

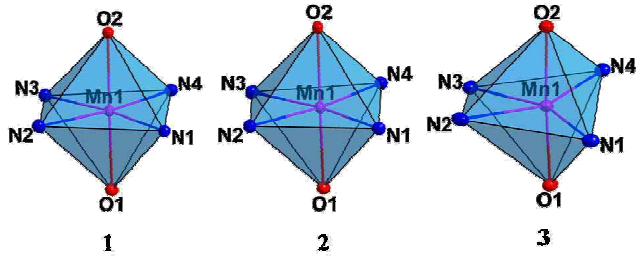

Fig. 4 Comparison of the configuration of octaherally coordinated Mn^{III} ions in complex **1**, **2** and **3** at 296 K.

Dalton Transactions Accepted Manuscript

Table 3 Selected bond distances (Å) and angles (°) for **3** at 296 K.

Bond Distances (Å)			
Mn(1)-O(1)	1.866(2)	Mn(1)-O(2)	1.872(2)
Mn(1)-N(1)	2.101(3)	Mn(1)-N(2)	2.262(4)
Mn(1)-N(3)	2.257(3)	Mn(1)-N(4)	2.124(3)
Ni(1)-S(1)	2.1637(10)	Ni(1)-S(2)	2.1603(11)
Ni(1)-S(6)	2.1605(11)	Ni(1)-S(7)	2.1553(11)
S(1)-C(1)	1.716(3)	C(1)-C(2)	1.359(5)
C(1)-S(3)	1.744(4)	S(3)-C(3)	1.731(4)
C(3)-S(5)	1.651(4)	C(3)-S(4)	1.712(4)
C(2)-S(4)	1.738(4)	C(2)-S(2)	1.713(4)
C(4)-S(6)	1.717(4)	C(4)-C(5)	1.358(5)
C(4)-S(8)	1.739(4)	C(5)-S(7)	1.711(4)
C(6)-S(8)	1.733(4)	C(6)-S(9)	1.723(5)
C(6)-S(10)	1.632(4)		
Bond Angles (°)			
O(1)-Mn(1)-O(2)	176.91(11)	O(1)-Mn(1)-N(1)	87.34(10)
O(2)-Mn(1)-N(1)	91.18(10)	O(1)-Mn(1)-N(4)	91.69(11)
O(2)-Mn(1)-N(4)	86.57(10)	N(1)-Mn(1)-N(4)	117.15(12)
O(1)-Mn(1)-N(3)	86.66(12)	O(2)-Mn(1)-N(3)	95.64(12)
N(1)-Mn(1)-N(3)	159.48(13)	N(4)-Mn(1)-N(3)	82.64(13)
O(1)-Mn(1)-N(2)	97.55(13)	O(2)-Mn(1)-N(2)	84.97(12)
N(1)-Mn(1)-N(2)	83.63(14)	N(4)-Mn(1)-N(2)	157.73(13)
N(3)-Mn(1)-N(2)	77.74(15)		
S(7)-Ni(1)-S(2)	86.14(4)	S(7)-Ni(1)-S(6)	92.80(4)
S(2)-Ni(1)-S(6)	175.79(5)	S(7)-Ni(1)-S(1)	177.85(5)
S(2)-Ni(1)-S(1)	93.04(4)	S(6)-Ni(1)-S(1)	88.15(4)
C(1)-S(1)-Ni(1)	102.30(12)	C(2)-S(2)-Ni(1)	102.09(12)
C(3)-S(3)-C(1)	97.25(18)	C(3)-S(4)-C(2)	97.67(17)
C(4)-S(6)-Ni(1)	102.24(13)	C(5)-S(7)-Ni(1)	102.83(13)
C(6)-S(8)-C(4)	97.76(19)	C(6)-S(9)-C(5)	98.01(19)
C(2)-C(1)-S(1)	120.8(3)	C(2)-C(1)-S(3)	115.6(3)
S(1)-C(1)-S(3)	123.6(2)	C(1)-C(2)-S(2)	121.7(3)
C(1)-C(2)-S(4)	116.1(3)	S(2)-C(2)-S(4)	122.2(2)
S(5)-C(3)-S(4)	122.4(2)	S(5)-C(3)-S(3)	124.2(2)
S(4)-C(3)-S(3)	113.4(2)	C(5)-C(4)-S(6)	121.3(3)
C(5)-C(4)-S(8)	115.9(3)	S(6)-C(4)-S(8)	122.8(2)
C(4)-C(5)-S(7)	120.8(3)	C(4)-C(5)-S(9)	115.8(3)
S(7)-C(5)-S(9)	123.4(2)	S(10)-C(6)-S(9)	123.5(2)
S(10)-C(6)-S(8)	123.9(3)	S(9)-C(6)-S(8)	112.5(2)

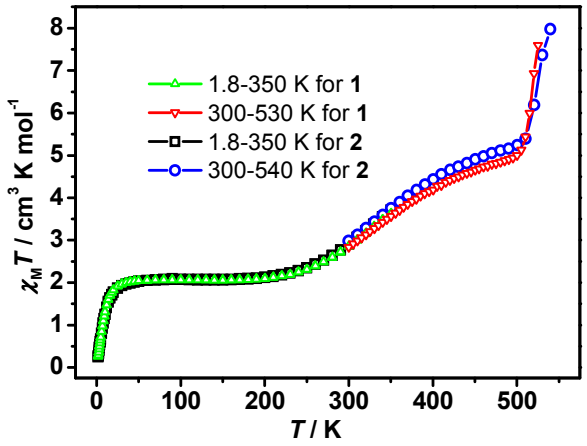

Fig. 5 Temperature dependence of $\chi_M T$ production of complexes **1** and **2**.

Magnetic properties and Theoretical calculations

Magnetic properties of 1 and 2. The temperature dependence of magnetic susceptibilities for **1** and **2** is shown in Fig. 5. Very clearly, **1** and **2** exhibit the almost same magnetic properties below 300 K and show slight differences above 300 K, so the property of complex **1** is mainly described in detail. As Fig. 4 displayed, the data above 500 K for **1** shows breakdown of the sample because the sample begins decomposed (the completely decomposed temperature is about 538 K observed in the TG plot as shown Fig. S2 for **1**). At 500 K, $\chi_M T$ value is 5 cm^3 K mol^{-1} for **1**, which is lower than completely HS value for two Mn^{III} ions (6 cm^3 K mol^{-1} for $S = 2$, $g = 2$), where $[Ni(mnt)_2]^{2-}$ is diamagnetic. With the temperature decreasing, the $\chi_M T$ value slowly decreases to a plateau at about 2.05 cm^3 K mol^{-1} between 170 K to 40 K, which is consistent with the expected value for two LS Mn^{III} ions (2 cm^3 K mol^{-1} for $S = 1$, $g = 2$). Below 40 K the $\chi_M T$ value decreases very quickly as a result of zero field splitting of Mn^{III} and/or intermolecular interactions. Therefore, the $\chi_M T$ plot suggests **1** and **2** undergo a analogous spin-crossover phenomenon. However, the calculated molar fraction of HS molecules is only 75% at 500 K, because of the breakdown of the sample, the step of completely HS phase could not be observed. Additionally, the calculated $\chi_M T$ value of $T_{1/2}$ should be 4 cm^3 K mol^{-1}. Therefore, the corresponding $T_{1/2}$ is 380 K. Compared with the reported **[**Mn(5-Br-sal-N-1,5,8,12)]ClO_4, $T_{1/2}$ has increased about 230 K. As the structural description above for complex **1**, the configuration of Mn^{III} shows the elongated metal-ligand bonds in equatorial plane with the temperature increasing. Correspondingly, when the complexes are heated enough, the *d* orbitals population should be changed (as displayed in Fig. 4), the complexes would like to HS state. In fact, the structural equatorial elongation is in good consistent population of the antibonding $d_{x^2-y^2}$ orbital upon switching to the HS state.[46] In a word, complexes **1** and **2** undergo a thermal SCO property. Additionally, in the reported complex **[**Mn(5-Br-sal-N-1,5,8,12)]ClO_4, one of the two cations exhibits SCO behavior. Herein, the replacement of $[M(mnt)_2]^{2-}$ make the two cations being the same geometric configuration, so both cations show SCO. The another reason is that $[M(mnt)_2]^{2-}$ (M = Ni, Pt) as counteranions disturb the subtle balance between enthalpy and entropy factors, the SCO phenomenon is largely influenced by the cooperativity.[47]

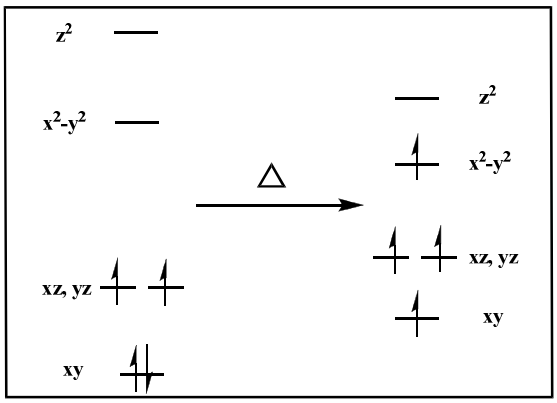

Fig. 6 Orbital population (*d* orbitals) for the $S = 1$ and $S = 2$ states of **1** and **2**.

Magnetic properties and theoretical study for 3. As shown in Fig. 7, at room tempetature the $\chi_M T$ value is 6.90 cm^3 K mol^{-1}, which is slightly higher than the expected value 6.75 cm^3 K mol^{-1}

Dalton Transactions Accepted Manuscript

This journal is © The Royal Society of Chemistry [year]

for two HS Mn^{III} ions (for one Mn^{III} ion: 3 cm^3 K mol^{-1} with S = 2, g = 2) and two $[Ni(dmit)_2]^-$ (for one Ni^{III} ion : 0.375 cm^3 K mol^{-1} with S = 1/2, g = 2). With temperature decreasing, the $\chi_M T$ value keeps a constant until to 50 K and quickly decreases reaching a minimum of 5.872 cm^3 K mol^{-1} at 9 K, which may attributed to the zero field splitting arising from Mn^{III} ions and/or the antiferromagnetic coupling exchanged from π-π interactions. With the further cooling, $\chi_M T$ increases a little to 5.898 cm^3 K mol^{-1} at 6 K, and then sharply goes down to 3.186 cm^3 K mol^{-1} at 1.8 K. Obviously, complex **3** does not exhibit SCO property. It could be ascribed to the significant Jahn-Teller distortions of Mn^{III} ion (Fig. 4). Therefore, complex **3** favors HS. Moreover, $[Ni(dmit)_2]^-$ as a counteranion influences on the geometric configuration of the cation in a great degree via weak interactions. At about 8 K the small increase of $\chi_M T$ value is mainly attributed to the existence of net spins ($S = \Sigma(S_{Mn} - S_{Ni}) = 3$). The sharp decreases at low temperature is due to the intermolecular antiferromangetic interactions.

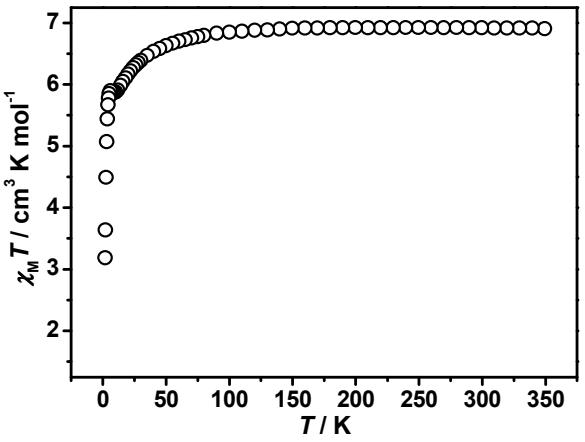

Fig. 7 Temperature dependence of $\chi_M T$ production of complex **3**.

We attempted to fit the magnetic data of complex **3** using several models with antiferromagnetic coupling J, zero-field splittling D of Mn^{III} ion and intermolecular interaction zj', but could not obtain the reasonable results because the three parameters all affect the magnetic properties in the same way and interfere each other in the fitting.[48] In order to evauate theoretically the coupling constant and the zero-field splitting parameters of Mn^{III}, we carried out the electronic structure calculation based on hybrid functional theory B3LYP and ab initio method CASPT2, respectively, for complex **3**. As revealed by structure analysis, the p-π interactions are weaker than π-π interactions, so an approximate magnetic system is suggested a tetranuclear Mn_2Ni_2 subunit [see Fig. 6(a)]. The calculated coupling constant J mediated through π-π interactions using B3LYP is −0.31 cm^{-1}, which indicates very weak antiferromagnetic coupling between Mn^{III} ion and the delocalized spins in $[Ni(dmit)_2]^-$. Furthermore, the field dependence of magnetization of complex **3** (Fig. S7 in ESI) recorded at 1.8 K could also support the above result. At 70 kOe, the value of magnetization is 6.51 $N\mu_B$, which is much lower than that of ferromagnetic coupling (10 $N\mu_B$) for two S = 2 and two S = 1/2 and close to the paramagnetic ground state due to the very weak antiferromagnetic coupling. As displayed in Fig. 6 (b), spin density distribution map in the low-spin state also proves the existence of antiferromagnetic couplings in complex **3**. Moreover, the calculated magnetic anisotropic parameters D and E values of the Mn^{III} fragment using CASPT2 are 4.96 cm^{-1} and −0.52 cm^{-1}, respectively. This D value is in the range of ones found in similar Mn complexes.[49-50] The Mn^{III} fragment has an easy plane [51-52] type of magnetic anisotropy.

In addition, the π-π stacking antiferromagnetic coupling can be illustrated by means of McConnell's theory [53] based on spin polarization effects. The reason of stabilization of the ferromagnetic interactions for intermolecular contacts in molecular $NH_4Ni(mnt)_2 \cdot H_2O$ has been explained by this mechanism.[54] This theory was also used to explain ferromagnetic interaction of complex $[Mn(Cp^*)_2]^+[Ni(dmit)_2]^-$ successfully.[55] Based on McConnell's theory, ferromagnetic interaction results from that the positive spin density of a unit interacts with the negative spin density of the adjacent unit dominantly, whereas antiferromagnetic coupling arises from dominant interaction between spin densities of the same sign. Table S4 (in ESI) displays the spin density population of the tetranuclear model (see Fig. S5 in ESI). As shown in Table S3, the absolute spin density population on Ni^{III} ions are very small, which suggests that a part of unpaired electrons have localized on the other atoms of the planar π-conjugated $[Ni(dmit)_2]^-$. All of the four pairs of atoms in the π-π stacking area (S89···C34, C38···S78, S95···C7, S72···C3) exhibit positive-positive spin density interactions. Obviously, following McConnell's theory π-π interaction mediates antiferromagnetic coupling. In a word, according to these analysis, there are antiferromagnetic interactions between Mn^{III} ion and the delocalized spins in $[Ni(dmit)_2]^-$.

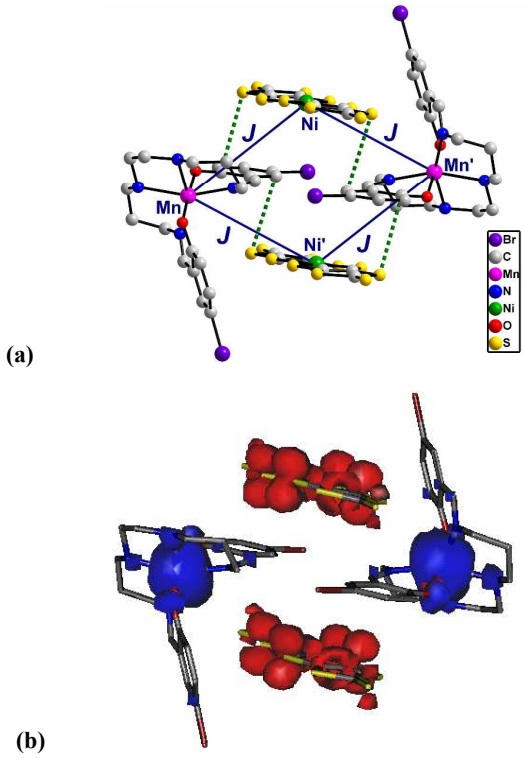

Fig. 8 (a) Representation of magnetic couplings in complex **3**. (b) Spin density distribution map of complex **3** in the low-spin state (blue and red regions indicate positive and negative spin populations, respectively; the isodensity surface represented corresponds to a value of 0.002 e^- $bohr^{-3}$).

Dalton Transactions Accepted Manuscript

Conclusion

Metal dithiolene complexes as counteranions, because of their planar π-conjugated structure, could affect the cooperativity of SOC complexes in different extent. When SCO cation $[Mn(5\text{-}Br\text{-}sal\text{-}N\text{-}1,5,8,12)]^+$ is hybrided with $[M(mnt)_2]^{2-}$ (M = Ni, Pt), the reaction forms two complexes **1** and **2**. Through the analysis of the metal-ligand bonds at five temperature and temperature dependence of magnetic susceptibilites, we could draw a conclusion that **1** and **2** show SCO phenomenon with higher $T_{1/2}$. However, when the cation reacted with $[Ni(dmit)_2]^-$ leading to the formation of complex **3** which does not show SCO property. Theoretical calculations show that π-π interactions mediate the antiferromagnetic coupling between Mn^{III} and Ni^{III} ions. Complex **3** contains π-π and p-π interactions, this kind of weak interactions perturb the configuration of Mn^{III} and hence orbital population, so complex **3** favors HS state. The change in metal-ligand bond length is an important driving force for SCO. Different metal dithiolene anions perturb the configuration of $[Mn(5\text{-}Br\text{-}sal\text{-}N\text{-}1,5,8,12)]^+$ cation in different ways, so three complexes show their characteristic features each.

Acknowledgements

This work was supported by Major State Basic Research Development Program (2013CB922102 and 2011CB808704), National Natural Science Foundation of China (21171089, 91022031 and 21021062), Natural Science Foundation of Jiangsu Province of China (BK2011778 and BK20130054).

Notes and references

[a]*State Key Laboratory of Coordination Chemistry, Nanjing National Laboratory of Microstructures and School of Chemistry and Chemical Engineering, Nanjing University, Hankou Road 22, Nanjing, 210093, P. R. China. Fax: +86 25 83314502; Tel : +86 25 83593739; E-mail: yousong@nju.edu.cn.*

[b]*School of Physical Science and Technology, Nanjing Normal University, Nanjing, 210097, P. R. China. E-mail: zhangyiquan@njnu.edu.cn.*

† Electronic Supplementary Information (ESI) available: Crystal structural data and refinement parameters for **2**; Octahedral structural parameters of Mn^{III} for $[Mn(5\text{-}Br\text{-}sal\text{-}N\text{-}1,5,8,12)]ClO_4$ and complexes **1**-**3**; Selected bond distances and angles for complex **2**; Comparison of Mn—N and Mn—O bond lengths at five collection temperatures in complex **2**; The TG plot of complexes **1**-**3**; Calculated atomic spin population for the tetranuclear model in complex **3**; The corresponding model for calculated atomic spin population for complex **3**; Details of hydrogen bonds for complex **3**; Field dependence of magnetization at 1.8 K for complex **3**; The IR spectrum of complexes **1**-**3**. CCDC reference numbers: 969625 for **1-123**, 976200 for **1-296**, 976201 for **1-350**, 976202 for **1-400**, 976203 for **1-473**, 969626 for **2-123**, 976204 for **2-296**, 976205 for **2-350**, 976206 for **2-400**, 976207 for **2-473**, 969627 for **3**.

1. P. Gutlich, V. Ksenofontov and A. Gaspar, *Coord. Chem. Rev.,* 2005, **249**, 1811-1829.
2. P. Gutlich, A. Hauser and H. Spiering, *Angew. Chem. Int. Ed. Ehgl.,* 1994, **33,** 2024-2054.
3. N. Shimamoto, S. Ohkoshi, O. Sato, and K. Hashimoto, *Inorg. Chem.,* 2002, **41**, 678-684.
4. M. Nihei, L. Han and H. Oshio, *J. Am. Chem. Soc.*, 2007, **129**, 5312-5313.
5. O. Kahn and C. J. Martinez, *Science*, 1998, **279**, 44-48.
6. O. Kahn and J. P. Launay, *Chemtronics*, 1988, **3**, 140.
7. M. E. Itkis, X. Chi, A. W. Cordes and R. C. Haddon, *science*, 2002, **296**, 1443-1445.
8. J. L. Brusso, O. P. Clements, R. C. Haddon, M. E. Itkis, A. A. Leitch, R. T. Oakley, R. W. Reed and and J. F. Richardsonlc, *J. Am. Chem. Soc.*, 2004, **126**, 8256-8265.
9. M. Sorai, M. Nakano and Y. Miyazaki, *Chem. Rev.*, 2006, **106**, 976.
10. J. Laugier, P. Rey, C. Benelli, D. Gatteschi and C. Zanchinilb, *J. Am. Chem. Soc.*, 1986, **108**.
11. P. J. Kunkeler, P. J. van Koningsbruggen, J. P. Cornelissen, A. N. van der Horst, A. M. van der Kraan, A. L. Spek, J. G. Haasnoot and J. Reedijk, *J. Am. Chem. Soc.*, 1996, **118**, 2190.
12. J. S. Miller and A. J. Epstein, *Chem. Commun.*, 1998, 1319-1325.
13. Z. Jie, J. Ensling, V. Ksenofontov, P. Gütlich, A. J. Epstein and J. S. Miller, *Angew. Chem. Int. Ed.,* 1998, **37**, 657.
14. W. Fujita and K. Awaga, *science*, 1999, **286**, 261-262.
15. R. Kato, *Chem. Rev.*, 2004, **104**, 5319-5346.
16. H.-B. Duan, X.-M. Ren and Q.-J. Meng, *Coord. Chem. Rev.,* 2010, **254**, 1509-1522.
17. M. Yamashita, N. Nakata, Y. Senshu, M. Nagata, H. M. Yamamoto, R. Kato, T. Shibauchi and Y. Matsuda, *Science*, 2010, **328**, 1246-1248.
18. J. M. Holland, J. A. McAllister, C. A. Kilner, M. Thornton-Pett, A. J. Bridgeman and M. A. Halcrow, *Dalton Trans.*, 2002, 548-554.
19. M. Nihei, H. Tahira, N. Takahashi, Y. Otake, Y. Yamamura, K. Saito and H. Oshio, *J. Am. Chem. Soc.,* 2010, **132**, 3553-3560.
20. C. Faulmann, S. Dorbes, B. Garreau de Bonneval, G. Molnár, A. Bousseksou, C. J. Gomez-Garcia, E. Coronado and L. Valade, *Eur. J. Inorg. Chem.,* 2005, 3261-3270.
21. S. Dorbes, L. Valade, J. A. Real and C. Faulmann, *Chem. Commun.*, 2005, 69-71.
22. C. Faulmann, S. Dorbes, S. Lampert, K. Jacob, B. Garreau de Bonneval, G. Molnár, A. Bousseksou, J. A. Real and L. Valade, *Inorg. Chim. Acta*, 2007, **360**, 3870-3878.
23. C. Faulmann, P. Á. Szilágyi, K. Jacob, J. Chahine and L. Valade, *New J. Chem.*, 2009, **33**, 1268.
24. C. Faulmann, K. Jacob, S. Dorbes, S. Lampert, I. Malfant, M.-L. Doublet, L. Valade and J. A. Real, *Inorg. Chem.*, 2007, **46**, 8548-8559.
25. M. F. Tweedle and L. J. Wilson, *J. Am. Chem. Soc.*, 1976, **98**, 4824.
26. K. Takahashi, H. Cui, H. Kobayashi, Y. Einaga and O. Sato, *Chem. Lett.*, 2005, **34**, 1240-1241.
27. K. Takahashi, H. Mori, H. Kobayashi and O. Sato, *Polyhedron*, 2009, **28**, 1776-1781.
28. S. Wang, M. Ferbinteanu, C. Marinescu, A. Dobrinescu, Q.-D. Ling and W. Huang, *Inorg. Chem.*, 2010, **49**, 9839-9851.
29. G. M. Sheldrick, *SADABSs: An Empirical Absorption Correction Program*, Bruker Analytical X-ray Systems, Madison, WI, 1996.
30. A. Patterson, *Phys. Rev.*, 1934, **46**, 372-376.
31. G. M. Sheldrick, *SHELXL-97, Program for refinement of crystal structures*, University of Göttingen, Germany, 1997.
32. E. L. Muetterties, *Inorganic Syntheses*, 1967, **X**, 11-16.
33. G. Steimecke, H.-J. Sieler, R. Kirmse and E. Hoyer, *Phosphorous and Sulfur and the Related Elements*, 1979, **7**, 49-55.
34. Neese, F. ORCA–*an ab initio, density functional and semiempirical program package*, version 2.9.1; Max-Planck institute for bioinorganic chemistry: Mülheim an der Ruhr, Germany, 2012.
35. A. D. Becke, *J. Chem. Phys*., 1993, **98**, 5648.
36. A. D. Becke, *Phys. Rev. A*, 1988, **38**, 3098.
37. C. Lee, W. Yang and R. G. Parr, *Phys. Rev. B*, 1988, **37**, 785.
38. F. Weigend and R. Ahlrichs, *Phys. Chem. Chem. Phys*., 2005, **7**, 3297.
39. G. Karlström, R. Lindh, P.-Å. Malmqvist, B. O. Roos, U. Ryde, V. Veryazov, P.-O. Widmark, M. Cossi, B. Schimmelpfennig, P. Neogrady and L. Seijo, *Comput. Mater. Sci*., 2003, **28**, 222.
40. J. S. Zhang, Q. Y. Zhu, D. X. Jia, J. Dai and D. Q. Zhang, *Synthesis and Reactivity in Inorganic, Metal-Organic, and Nano-Metal Chemistry*, 2005, **35**, 633-637.
41. W.-B. Pei, J.-L. Liu, J.-S. Wu, X.-M. Ren, D.-W. Gu, L.-J. Shen and Q.-J. Meng, *J. Mol. Struct.*, 2009, **918**, 160-164.

Dalton Transactions Accepted Manuscript

This journal is © The Royal Society of Chemistry [year]

42. W.-B. Pei, J.-S. Wu, J.-L. Liu, X.-M. Ren and L.-J. Shen, *Spectrochim. Acta Part A: Molecular and Biomolecular Spectroscopy*, 2010, **75**, 191-197.
43. H. Bois, N. G. Connelly, J. G. Crossley, J.-C. Guillorit, G. R. Lewis, A. G. Orpen and P. Thornton, *J. Chem. Soc., Dalton Trans.,* 1998, 2833-2838.
44. M. Bousseau, L. Valade, J.-P. Legros, P. Cassoux, M. Garbaukas and L. V. Interrante, *J. Am. Chem. Soc.*, 1986, **108**, 1908-1916.
45. B. Pomarède, B. Garreau, I. Malfant, L. Valade, P. Cassoux, J.-P. Legros, A.Audouard, L. Brossard, J.-P. Ulmet, M.-L. Doublet and E. Candell, *Inorg. Chem.*, 1994, **33**, 3401-3414.
46. G. G. Morgan, K. D. Murnaghan, H. Müller-Bunz, V. McKee, and C. J. Hardin, *Angew. Chem. Int. Ed.*, 2006, **45**, 7192-7195.
47. O. Kahn, *Molecular Magnetism*, 1993, 59-82.
48. A. Panja, P. Guionneau, I.-R. Jeon, S. M. Holmes, R Clérac, and C. Mathonière, *Inorg. Chem.*, 2012, **51**, 12350.
49. M. Retegan, M.-N. Collomb, F. Neese and C. Duboc, *Phys. Chem. Chem. Phys.*, 2013, **15**, 223.
50. M. Corbella, R. Costa, J. Ribas, P. H. Fries, J.-M. Latour, L. Öhrström, X. Solans and V. Rodríguez, *Inorg. Chem.*, 1996, **35**, 1857-1865.
51. B. A. Ivanov and E. V. Tartakovskaya, *Phys. Rev. Lett.*, 1996, **77**, 386..
52. V. A. Chernenko, V. A. Lvov, S. Besseghini and Y. Murakami, *Scripta Materialia*, 2006, **55**, 307-309.
53. H. M. McConnell, *J. Chem. Phys.* 1963, **39**, 1910.
54. A. T. Coomber, D. Beljonne, R. H. Friend, J. L. Brédas, A. Charltom, N. Robertson, A. E. Underhill, M. Kurmoo and P. Day, *Nature*, 1996, **380**, 144-146.
55. C. Faulmann, E. Rivie‘re, S. Dorbes, F. Senocq, E. Coronado, P. Cassoux, *Eur. J. Inorg. Chem.*, 2003, 2880.

Dalton Transactions Accepted Manuscript

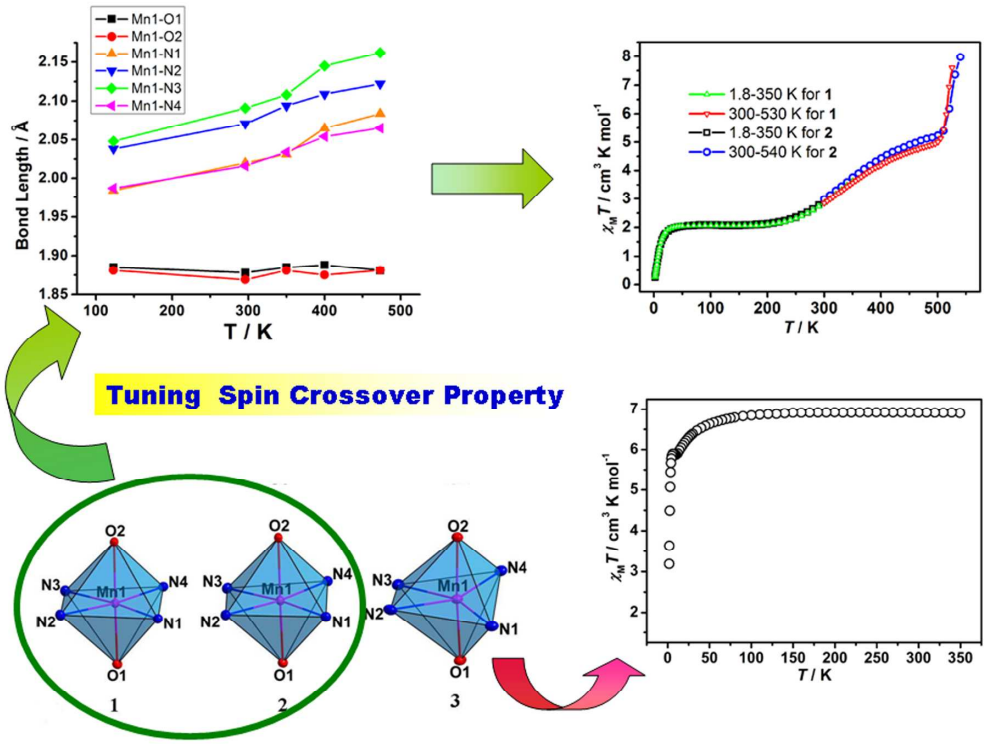

Different metal dithiolene anions affect the configuration of $[Mn(5\text{-Br-sal-N-1,5,8,12})]^+$ cation in different ways, so three complexes show their characteristic features each.

Dalton Transactions Accepted Manuscript